Heliyon 9 (2023) e15727

Contents lists available at ScienceDirect

Heliyon

journal homepage: www.cell.com/heliyon

Research article

Navigation of a compartmentalized robot system

Bibhya Sharma, Riteshni D. Karan, Sandeep A. Kumar *, Avinesh Prasad

School of Information Technology, Engineering, Mathematics and Physics, The University of the South Pacific, Fiji

A R T I C L E   I N F O

MSC:
00-01
99-00

Keywords:
Motion control
Compartmentalization
Efficient variant
Car like robot
Minimum distance technique
Globally rigid formation

A B S T R A C T

After making progression in developing the fundamental problems related to single-robot control, many researchers swerved and diverged their focus to studying multi-robot coordination. This research aims to take the motion planning and control (MPC) problem of a multi-robot system into a new space by considering a compartmentalized robot. An efficient variant of globally rigid formation, in which multiple car-like units are adjoint and move in parallel without collisions. The motion is governed by one of the sub-units acting as a leader, while other units maintain the fixed distance amongst each other and the leader in a rigid formation. The minimum distance technique is an important input to facilitate collision avoidance, robot decision making, and robot navigation. In this study a novel method to analytically compute the minimum distance between the closest point on the line segments of rectangular protective region and the obstacle is presented. Utilizing the Lyapunov-based Control Scheme a set of autonomous controllers are designed. Computer simulations of the proposed Lyapunov-based controllers for the compartmentalized robot are presented in interesting scenarios to show the efficacy of the unique set of controllers. In these simulations, the compartmentalized robot shows strict maintenance of a rigid formation with efficient collision and obstacle avoidance. The results open up research in the design and implementation of controllers by considering multiple compartmentalized robots into swarm models, splitting and re-joining units, and applying rotational leadership ideas.

1. Introduction

Navigation is an essential factor in mobile robotics involving faultlessly identifying the robot's position, planning the path, and following the planned path [1]. Localization is the robot's ability to determine its location in the real world to its position within a map; Path planning is the calculation of a path through a map representing the environment. This predetermined path is chosen based on the problem goals to achieve the expected target. Therefore, a reliable map is essential for navigation, without which robots cannot reach their destinations. The reliability of the map is challenging in navigation problems due to the dynamic and unpredictable nature of real-world applications [2,1].

Robots perform jobs that are too dirty, dangerous or dull to be suitable for humans [3]. They are universally employed in areas such as mass production [4], assembling [5], packaging [6], transport [7], rescue [8], earth and space study [9], medical [10], and field artillery [11]. There has been a lot of work carried out on improvements of the robotic performance. A single robot's performance can be limited to its inability to coordinate, communicate, and understand its actions, roles, and task status, reducing its

* Corresponding author.
E-mail address: sandeep.a.kumar@usp.ac.fj (S.A. Kumar).

https://doi.org/10.1016/j.heliyon.2023.e15727
Received 30 May 2022; Received in revised form 12 April 2023; Accepted 19 April 2023

Available online 23 April 2023
2405-8440/© 2023 The Authors. Published by Elsevier Ltd. This is an open access article under the CC BY-NC-ND license (http://creativecommons.org/licenses/by-nc-nd/4.0/).

usefulness in applications where tasks cannot be performed by a single robot [12]. To cope with the complex tasks, multiple robots with different levels of capacities and formations have been frequently deployed [13,14].

Using multiple robots over single robots has both practical and theoretical advantages in different circumstances. These include desired performance with tight time and cost constraints, increased robustness, fault tolerance, better security and capabilities[15, 16]. In certain situations physical limitations and computational issues such as role and task allocations may arise. Therefore, researchers are constantly designing efficient task or behavior-based algorithms for multiple robot systems under various conditions and levels of formation [17].

In formation control the posture of a team of robots is controlled while preserving their geometrical structure and permitting them to travel to their destinations [18–20]. Surveillance, transportation, health-care, exploration and rescue are some of its applications. Formation by the pattern is motivated by cooperative behavior observed in nature, such as swarming ants, flocking of birds, schooling of fish, and herding of animals [17]. The four layers of formation control are formation shape, formation type, formation tracking, and robot roles. Various approaches are addressed in the literature on the problem of formation control in robotic applications. Namely, these approaches can be categorized as leader-follower, virtual structure, generalized coordinates, behavior-based, and social potential fields. A detail account of the approaches mentioned above is well-presented in [21–23,3,20]. One of the challenges in controlling the formation is maintaining the rigidness of the patterns formed by the multiple robots. Split/rejoin allows for uncontrolled changes to the formation pattern, while in globally rigid formation it is essential to have a strict maintenance of the formation. In locally rigid formation the formation patterns are temporarily distorted while encountering obstacles and restrictions [17]. Novel applications of formation control include [21].

The two main approaches of motion planning and control algorithms of multiple robots are classical algorithms and heuristic algorithms [24]. Classical algorithm includes the establishment of roadmaps [25], cell dismantling [26], reactive approaches namely, fuzzy logic [27], neural networks [28], and neuro-fuzzy systems [29] and the artificial potential field (APF) method [30]. In many applications some of these can be combined with heuristic algorithms to derive the most effective route planning method [31]. This research considers the Lyapunov based Control Scheme (LbCS), which falls under APF methodology, for motion planning and control (MPC) of compartmentalized multiple agents.

In LbCS, the movement of the robot in the surrounding space is converted into the virtual force field movement. The target point attracts the robot towards it, the repulsive force of the obstacles averts the robot from moving towards them. The resulting force is the combination of the attractive force of the target and the repulsive force of all obstacles. The magnitude and direction of the resultant force determines the state and motion of the robot. The LbCS has been successfully applied in the literature to find feasible and stabilizing solutions to a variety of problems [17]. This paper introduces a set of nonlinear time-invariant control laws through a fusion of the LbCS and a leader-follower scheme to mobilize a compartmentalized robot while maintaining a globally rigid formation. The two restrictions of the approach are; first, it has the disadvantages of APFs, particularly the local minima, and second, the poor disturbance rejection properties and dependency on the leader of the leader-follower scheme. Nevertheless, the novelty of the new approach lies in the ability to design control laws to formulate globally rigid formations of nonholonomic systems affixed by dynamic constraints. The LbCS controllers are practical and easy to construct compared to the mathematically and computationally exhaustive ones found in the literature. LbCS has a built-in process to turn these constraints into artificial obstacles and integrate them into the controllers. Finally, the association of the new leader-follower scheme facilitates various tasks compared to purely cooperative agents. One advantage of the proposed scheme is using Cartesian coordinate representations to avoid encountering singular points compared to polar coordinates. Another advantage is assigning a single target for a group of car-like robots via a new leader-follower approach. The framework is a leader-follower scheme for compartmentalized robots to establish, maintain and translate the entire team in a rigid formation around the workplace, performing a specific task through centralized control laws.

1.1. Contributions

This paper presents a unique variant of formation control by considering a compartmentalized robot system in a constrained environment using an integration of the Lyapunov-based control scheme (LbCS) and the centralized leader-follower design. The LbCS, which is a type of artificial potential field (APF) is deployed in various applications for numerous robotic systems including holonomic or nonholonomic constraints. The LbCS is vastly used over other motion control paradigms because mathematical functions related to limitations, inequalities and other mechanical restrictions associated with the robotic system are easier to construct and integrate into the controllers derived.

The motion planning and control problem is taken into a new dimension by introducing the concept of compartmentalized robot which is invariably capable of multi-tasking. Here the robot is compartmentalized into smaller units and maneuvered in parallel without collision whilst maintaining the formation with the help of a pre-determined subunit which acts as the leader. The advantage of using compartmentalized robot system is its relative low cost and the fact that it takes up less space in the workspace [32–34].

The contributions of this paper are presented as follows:

- **(i)** Mathematical integration of the LbCS and leader-based control schemes to address the MPC of a compartmentalized robot system.
- **(ii)** The minimum distance technique adapted in obstacle avoidance by utilizing the rectangular protective region of the subunits.

(iii) Designing of a set of new nonlinear time-invariant acceleration based control laws according to LbCS for collision - free movements of a compartmentalized robotic system.

(iv) MPC of a compartmentalized robotic system, governed by one of the subunits as a centralized leader to the designated target. This classifies a compartmentalized robot system as a variant of global rigid formation where convergence of the system to the target is attained by a virtual leader.

The paper is organized as follows: In section 2, the kinematic model of the compartmentalized robot is described in detail; section 3 defines the APF functions. The Lyapunov function is constructed, and the nonlinear continuous controllers for the mobile robot are excerpted in section 4. Section 5 discusses the stability of the system. In section 6, the simulation results are shown to prove the robustness and effectiveness of the proposed controller input, followed by the conclusion in section 7.

1.2. Related works

The development of compartmentalized systems in the recent years has led to innovative strategies ranging from macroscopic approaches via temporal and spatial compartmentalization to microscopic approaches based on nonvectors [35]. The profound study of such systems is in areas such as synthetic biology, materials science, protein and medical engineering [36], modern surgical procedure and acupuncture [37], collection and transportation of wastes [32], and crop treatments in agriculture [33]. Scientists have also invented robots that 'team up' to form larger robots. The research led by Marco Dorigo of the University Libre de Buxelles' IRIDIA AI intelligence lab, focused on getting robots to behave as independent units by default, but also join forces and become a single machine when required [38]. As the robots merge into one unit, they hand off control over themselves to the single "main" robot. The main robot is then responsible for the actions of the newly formed, larger robot. The control paradigm enabled robots to demonstrate properties beyond any existing machine or biological organism. The robots presented; unify to form larger bodies with a single centralized controller, split into separate bodies with independent controllers, and self-heal by removing or replacing malfunctioning body modules [38]. A team of researchers from Georgia Institute of Technology and Northwestern University developed a modular system of smaller robots. A robot made of other rudimentary robots called smart active particles (smarticles) [39]. The tiny form of these robots can be used in extraction team operations. For example, sensor-equipped units spread over the wreckage of a subsided house to find the victims buried underneath the debris. A whole swarm of these tiny robots could assemble to create a temporary bridge over a waterway [39]. Minuscule units also can be used to convey drugs to hard-to-reach parts of a human body or improve research on modeling the cellular action involved in organ formation [38]. While the concept of compartmentalization has been utilized in synthetic biology, materials science, medical engineering, collection and transportation and in agriculture, this is first time compartmentalized robot system has permeated into a motion planning and control problem.

Numerous papers have studied motion planning and control of different robotic systems in formation such as mobile manipulators, articulated robotic arm, a wheeled platform, and swarms of homogeneous or heterogeneous systems. This paper includes an unused concept of compartmentalized robot which is an efficient variant of globally rigid formation. In this research, the compartmentalized robot has 4 separated units, adjoint, meaning that all units are bounded mathematically as an automated intelligent machine in a rigid formation, controlled via the Lyapunov-based control scheme. The advantages include satisfactorily completion of multiple tasks which are not feasible with simple cooperative agents, high energy efficiency, and decrease in overall costs [40].

1.3. The Lyapunov-based control scheme

This research uses the Lyapunov-based control scheme (LbCS), is applied widely in robotics, especially in the analysis of motion planning and control problems [41–43]. It is a type of Artificial Potential Field method that uses the Lyapunov function or total potentials to design appropriate velocity or acceleration-based controllers that guide the robots to their designated goals.

The controllers, which are the translational and rotational accelerations are designed such that the compartmentalized robot will be able to carry out subtasks before reaching its destination are also designed accordingly. The subtasks include navigation of the static environment while adhering to the kinematic and dynamic constraints and safely making it to the target position in a rigid formation. The proposed potential functions are fundamentally the distance functions formed in Euclidean space, a strategy often cited in the literature. The Lyapunov-based control scheme suitably integrates these potential field functions to devise a Lyapunov function - a platform for designing the nonlinear controls for the mobile robots.

In Fig. 1(a) a 3D view of the Lyapunov function or total potentials is shown while its corresponding contour plot is shown in Fig. 1(b). Fig. 1 is produced from the attractive function governed by (3) and the repulsive potential functions designed from (4) for the compartmentalized robot is presented.

2. System modeling

In this section, the kinematic model for compartmentalized robot is derived which consists of 4 homogeneous car-like units, adjoint in the Euclidean plane as shown in Fig. 2.

Definition 2.1. The compartmentalized robot A_0 is a mobile robot, sub divided into 4 smaller car - like robots, called units. Let A_0 be a rectangle with length $(2L + 4\epsilon_1)$ and width $(2l + 4\epsilon_2)$ with θ_1 as angle of orientation in the $z_1 z_2$ plane.

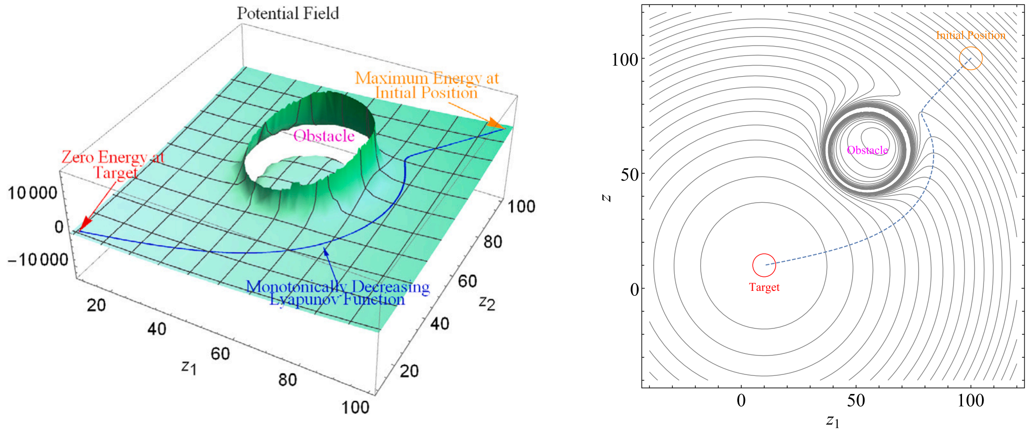

(a) 3D visualization (b) Contour Plot

Fig. 1. An illustration of total potentials and contour plot generated from LbCS.

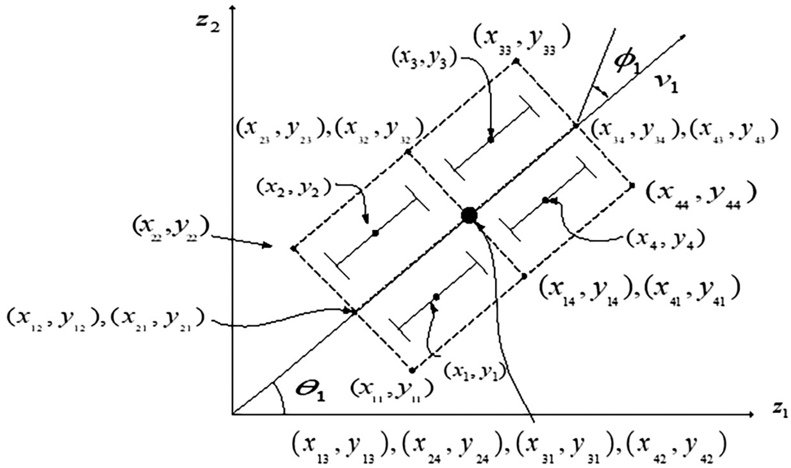

Fig. 2. Compartmentalized robot of adjoint car - like units with their protective regions.

Definition 2.2. The ith car - like unit A_i is a disk with radius r_i and positioned at the center (x_i, y_i). Precisely, the ith unit is the set

$$A_i = \{(z_1, z_2) \in \mathbb{R}^2 : (z_1 - x_i)^2 + (z_2 - y_i)^2 \leq r_i\}$$

for $i \in \{1, 2, 3, 4\}$.

Each unit A_i is assumed to be a rear wheel driven car-like mobile robot. Its engine power is applied to the rear wheels. Cartesian coordinates are used to derive the model to avoid injection of singularities that are unwanted into the navigation problem. Referring to Fig. 3, (x_1, y_1) indicates the center of mass of the leader unit A_1, θ_1 gives orientation and ϕ_1 denotes the steering wheels angle with respect to the z_2-axis. Here L acts for the distance between the centers of the front and the rear axles of the units and l the length of each axle. ϵ_1 and ϵ_2 are the clearance parameters. The coordinates for the center of mass of A_i, (x_i, y_i) in the compartmentalized robot are given by:

$$x_i = x_1 + \sum_{i=1}^{4} \left(2\left[\lceil \frac{i}{2} \rceil - \lceil \frac{i}{4} \rceil\right] \left(\frac{L}{2} + \epsilon_1\right) \cos\theta_i + \left[(-1)^{\lfloor \frac{i}{2} \rfloor} - 1\right] \left(\frac{l}{2} + \epsilon_2\right) \sin\theta_i \right),$$

$$y_i = y_1 + \sum_{i=1}^{4} \left(2\left[\lceil \frac{i}{2} \rceil - \lceil \frac{i}{4} \rceil\right] \left(\frac{L}{2} + \epsilon_1\right) \sin\theta_i - \left[(-1)^{\lfloor \frac{i}{2} \rfloor} - 1\right] \left(\frac{l}{2} + \epsilon_2\right) \cos\theta_i \right).$$

The kinematic model of the system which inherently captures nonholonomic constraints is described as:

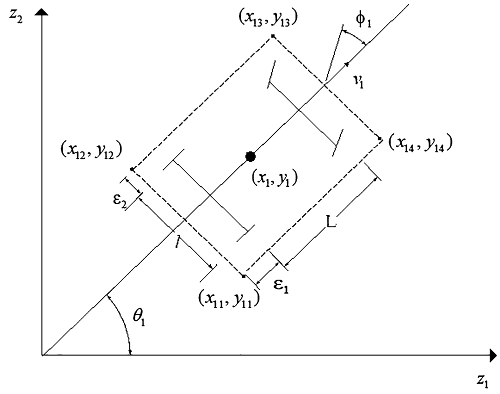

Fig. 3. A schematic diagram showing a rear wheel driven car like unit A_1 with steering angle ϕ_1.

$$\left.\begin{aligned}
&\dot{\theta}_i = \frac{v_i}{L}\tan\phi := \omega_i,\\
&\dot{v}_i = \sigma_{i1}, \omega^{\cdot}_i = \sigma_{i2},\\
&\dot{x}_i = v_1\cos\theta_1 - \frac{L}{2}\omega_1\sin\theta_1 - \sum_{i=1}^{4}\left(2\left[\lceil \tfrac{i}{2}\rceil - \lceil \tfrac{i}{4}\rceil\right]\left(\frac{L}{2}+\epsilon_1\right)\omega_i\sin\theta_i + \left[(-1)^{\lfloor \frac{i}{2}\rfloor} - 1\right]\left(\frac{l}{2}+\epsilon_2\right)\omega_i\cos\theta_i\right),\\
&\dot{y}_i = v_1\sin\theta_1 + \frac{L}{2}\omega_1\cos\theta_1 + \sum_{i=1}^{4}\left(2\left[\lceil \tfrac{i}{2}\rceil - \lceil \tfrac{i}{4}\rceil\right]\left(\frac{L}{2}+\epsilon_1\right)\omega_i\cos\theta_i - \left[(-1)^{\lfloor \frac{i}{2}\rfloor} - 1\right]\left(\frac{l}{2}+\epsilon_2\right)\omega_i\sin\theta_i\right), i \in \{1,2,3,4\}.
\end{aligned}\right\} \quad (1)$$

The orientation of A_i is given by θ_i with respect to the z_1-axis, the translational and rotational velocities are v_i and ω_i. The translational and rotational accelerations or the controllers of A_0 are σ_{i1} and σ_{i2}.

The nonholonomy of the car-like unit are the kinematic constraints and any fixed or moving obstacles in the workspace. The nonholonomy of the unit is emulated in the kinematic model (1). Disks or circles have been considered as the protective region around each robot. The protective regions ensure that each robot can steer itself safely when encountering or moving past an obstacle. In this research the protective region of the units is taken as a rectangle of coordinates (x_{in}, y_{in}), where i represents the ith unit and $n = 4$ line segments of the rectangular protective region around each A_i, with length of $(L + 2\epsilon_1)$ and width of $(l + 2\epsilon_2)$ as shown in Fig. 2 and Fig. 3, respectively.

The protective regions of the subunits of A_0 are constructed. First the coordinates of the vertices of the rectangular protective region for A_i are derived with respect to the center of mass (x_1, y_1) of the lead unit A_1.

$$x_{in} = x_1 + \left[(-1)^{\lceil \frac{i}{2}\rceil} + (-1)^{\lceil \frac{n}{2}\rceil} + 1\right]\left(\frac{L}{2}+\epsilon_1\right)\cos\theta_i + \left[(-1)^{\lfloor \frac{i}{2}\rfloor} + (-1)^{\lfloor \frac{n}{2}\rfloor} - 1\right]\left(\frac{l}{2}+\epsilon_2\right)\sin\theta_i,$$

$$y_{in} = y_1 + \left[(-1)^{\lceil \frac{i}{2}\rceil} + (-1)^{\lceil \frac{n}{2}\rceil} + 1\right]\left(\frac{L}{2}+\epsilon_1\right)\sin\theta_i - \left[(-1)^{\lfloor \frac{i}{2}\rfloor} + (-1)^{\lfloor \frac{n}{2}\rfloor} - 1\right]\left(\frac{l}{2}+\epsilon_2\right)\cos\theta_i.$$

The advantage of using a rectangular protective regions over circular ones is providing relatively more free space as shown in Fig. 4. The area enclosed in the workspace by the rectangular protective region with length $(L + 2\epsilon_1)$ and width $(l + 2\epsilon_2)$ is given by $A_{rectangle} = (L + 2\epsilon_1)(l + 2\epsilon_2)$. The area enclosed by the circular protective region of radius $r_v = \sqrt{(2\epsilon_1 + L)^2 + (2\epsilon_2 + l)^2}/2$ is given by $A_{circle} = \pi((2\epsilon_1 + L)^2 + (2\epsilon_2 + l)^2)/4$. Clearly, $A_{rectangle} < A_{circle}$. For an easier generalization, parametric equations of the line segments connecting the vertices of the protective region, as shown in Fig. 2, are derived with respect to A_1.

Definition 2.3. The nth boundary line of the protective region around the ith unit is a line segment in the z_1z_2-plane, from the point (x_{in}, y_{in}) to the point (x_{im}, y_{im}) (where $m = n + 1 - 4\lfloor n/4 \rfloor$). Precisely, the nth boundary line is the set:

$$BL_{in} = \{(z_1, z_2) \in \mathbb{R}^2 : (z_1 - X_{in})^2 + (z_2 - Y_{in})^2 = 0)\},$$

where $X_{in} = x_{in} + (x_{im} - x_{in})\lambda_{in}$ and $Y_{in} = y_{in} + (y_{im} - y_{in})\lambda_{in}$ are the parametric representations for $0 \leq \lambda_{in} \leq 1$, when $i, n = 1, 2, 3, 4$.

Consider the nth line segment in the z_1z_2 plane as per Definition 2.3. Assume that it is the boundary line of the protective regions and that points (x_{in}, y_{in}) where $i = n$ are the coordinates of the vertex of outer rectangular protective region of the compartmentalized robot, then from vector geometry, the parametric equations of the outer line segments of the rectangular protective region are:

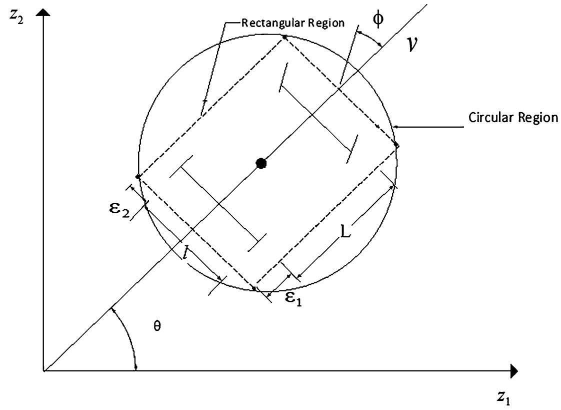

Fig. 4. A comparison of free space occupied in the workspace.

$$\left.\begin{aligned} X_{in} &= x_1 + \left[(-1)^{\lceil \frac{i}{2} \rceil} + (-1)^{\lceil \frac{n}{2} \rceil} + 1\right]\left(\frac{L}{2} + \epsilon_1\right)\cos\theta_i + \left[(-1)^{\lfloor \frac{i}{2} \rfloor} + (-1)^{\lfloor \frac{n}{2} \rfloor} - 1\right]\left(\frac{l}{2} + \epsilon_2\right)\sin\theta_i \\ &\quad + (-1)^{\lfloor \frac{n}{2} \rfloor}\left[2(1-(-1)^n)\left(\frac{L}{2} + \epsilon_1\right)\cos\theta_i - 2(1+(-1)^n)\left(\frac{l}{2} + \epsilon_2\right)\sin\theta_i\right]\lambda_{in}, \\ Y_{in} &= y_1 + \left[(-1)^{\lceil \frac{i}{2} \rceil} + (-1)^{\lceil \frac{n}{2} \rceil} + 1\right]\left(\frac{L}{2} + \epsilon_1\right)\sin\theta_i - \left[(-1)^{\lfloor \frac{i}{2} \rfloor} + (-1)^{\lfloor \frac{n}{2} \rfloor} - 1\right]\left(\frac{l}{2} + \epsilon_2\right)\cos\theta_i \\ &\quad + (-1)^{\lfloor \frac{n}{2} \rfloor}\left[2(1-(-1)^n)\left(\frac{L}{2} + \epsilon_1\right)\sin\theta_i + 2(1+(-1)^n)\left(\frac{l}{2} + \epsilon_2\right)\cos\theta_i\right]\lambda_{in}; \end{aligned}\right\} \tag{2}$$

where λ_{in} is a non-negative scalar, restricted to the interval $[0,1]$ only.

For example, when $i = n = 3$ the following parametric equation is obtained by taking the vertex coordinates (x_{33}, y_{33}) and (x_{22}, y_{22})

$$\begin{aligned} X_{33} &= x_1 + 3\left(\frac{L}{2} + \epsilon_1\right)\cos\theta_i - 3\left(\frac{l}{2} + \epsilon_2\right)\sin\theta_i - \left[4\left(\frac{L}{2} + \epsilon_1\right)\cos\theta_i\right]\lambda_{33}, \\ Y_{33} &= y_1 + 3\left(\frac{L}{2} + \epsilon_1\right)\sin\theta_i + 3\left(\frac{l}{2} + \epsilon_2\right)\cos\theta_i - \left[4\left(\frac{L}{2} + \epsilon_1\right)\sin\theta_i\right]\lambda_{33}. \end{aligned}$$

3. Research objective

In this research an efficient variant of globally rigid formation is prescribed as a compartmentalized robot A_0 with sub-unit A_1 as its leader. A globally rigid formation is defined as:

Definition 3.1. A globally rigid formation is a strictly maintained geometric pattern without any distortion to the prescribed formation in translation under any given circumstance.

Hence there is no need for a virtual leader which has been a compulsory component of globally rigid formation. The distance between the units within the formation is maintained throughout the motion. With A_1 as the leader, the task performed by A_0 in this paper is avoidance of obstacles, randomized in size, position and numbers. Main objective of the research is to design the potential field functions using the LbCS, and accordingly derive its non-linear acceleration based controllers, σ_{11} and σ_{12}, for the leader A_1, which will move A_0 towards the target in an obstacle ridden environment.

Problem of statement

Consider A_0 be a compartmentalized robot, with $A_i, i \in \{1,2,3,4\}$ as its compartments, as seen in Fig. 2, moving in a confined workspace in the $z_1 z_2$ plane. Allow $O_1, O_2, ..., O_k$ to be immobile circular obstacles, placed randomly in the workspace. Given an initial position and orientation of A_0, the controllers for the leader A_1 are derived so that it converges A_0 to a target while fulfilling the nonholonomic constraints and steer clear of $O_k, k \in \{1,2,...,k\}$.

This section will design appropriate attractive and repulsive potential field function in accordance with LbCS.

3.1. Potential field functions for the car-like units

In the compartmentalized robot A_0 the units A_i for $i \in \{2,3,4\}$ maintain a fixed distance amongst each other and from leader A_1. Due to fixed distance throughout the motion, the other units A_i do not require separate targets. They converge to a common target in unison with their leader A_1 in a rigid formation. The target for a car-like robot is defined as:

Definition 3.2. The target assigned for A_0 which is governed by the leader A_1 is a disk with center (P_{11}, P_{12}) and radius r_T. It is described as the set

$$T = \{(z_1, z_2) \in \mathbb{R}^2 : (z_1 - P_{11})^2 + (z_2 - P_{12})^2 \leq r_T^2\}.$$

The Euclidian distance between the position (x_1, y_1) of the leader A_1 and the target at time $t \geq 0$ is calculated for target attraction.

$$V(\mathbf{x}) = \frac{1}{2}[(x_1 - P_{11})^2 + (y_1 - P_{12})^2 + v_1^2 + \omega_1^2]. \tag{3}$$

The target attraction function is a measure of A_1's convergence to its target. Inclusion of the velocity components into the attraction function adds another dimension to the control laws.

The compartmentalized robot A_0's convergence to the target is facilitated by the leader A_1. Since the other units A_i for $i \in \{2, 3, 4\}$ are in a rigid formation with the leader, they also converge to the target at the same speed as A_1.

3.2. Convergence function of the car-like units

Auxiliary function

To ensure that the compartmentalized robot A_0 converges to its target and to guarantee that the controllers dissolve at the target, an auxiliary function $F(\mathbf{x})$ is constructed. The inverse of each avoidance function built is multiplied to $F(\mathbf{x})$[17]. Thus an approximate auxiliary function can be:

$$F(\mathbf{x}) = \frac{1}{2}[(x_1 - P_{11})^2 + (y_1 - P_{12})^2].$$

At the target center (P_{11}, P_{12}), the velocities v_i and ω_i will be zero to guarantee the units stops and take a desired final orientation.

3.3. The kinematic constraints

The nonholonomic properties and any fixed or moving obstacle in the workspace are the kinematic constraints of the mobile car-like robots. The fixed obstacles considered are stationary solid fixed objects within the workspace. Consider that the work space environment of the compartmentalized robot is cluttered with $k \in \mathbb{N}$ fixed obstacles. The compartmentalized robot has to avoid the fixed obstacles. The avoidance is through equations derived for the units A_i. The definition of the kth circular fixed obstacles for a car-like robot is adapted from the work of [44].

Definition 3.3. The kth fixed circular obstacle is a disk with center (o_{1k}, o_{2k}) and radius r_{ok}). The kth disk shaped obstacle, for $k \in \mathbb{N}$, is precisely a set

$$FO_k = \{(z_1, z_2) \in \mathbb{R}^2 : (z_1 - o_{1k})^2 + (z_2 - o_{2k})^2 \leq r_{ok}^2\}.$$

The minimum distance technique (MDT) introduced by Sharma et al. [17] will be applied for the avoidance of obstacles by the compartmentalized robot. MDT involves calculating the smallest distance between the center of the circular obstacle (o_{1k}, o_{2k}) to a nearest point on the outer line segments of the rectangular protective region of the compartmentalized robot A_0. The avoidance is by the closest point on the rectangular protective region at any point in time $t > 0$, resulting in the avoidance of the obstacle by the entire line segment. The advantage of using (MDT) is that only a single point on a line segment closest to the obstacle avoids the obstacle. This approach guarantees that the whole rectangular protective region of A_0 avoids the obstacle.

For MDT, take any point on the 8 outer line segments of (X_{in}, Y_{in}), defined in (2) and the fixed obstacle (o_{k1}, o_{k2}), and find the distance function $D_{in} = \sqrt{(X_{in} - o_{1k})^2 + (Y_{in} - o_{2k})^2}$. Differentiate D_{in} with respect to λ_{in}, to find λ_{in} so that D_{in} is minimum yields to:

$$\begin{aligned} \lambda_{in} &= \Big\{ o_{1k} - [x_1 + \Big[(-1)^{\lceil \frac{i}{2} \rceil} + (-1)^{\lceil \frac{n}{2} \rceil} + 1\Big] \left(\tfrac{L}{2} + \epsilon_1\right) \cos\theta_i + \Big[(-1)^{\lfloor \frac{i}{2} \rfloor} + (-1)^{\lfloor \frac{n}{2} \rfloor} - 1\Big] \left(\tfrac{l}{2} + \epsilon_2\right) \sin\theta_i] \\ &+ (-1)^{\lfloor \frac{n}{2} \rfloor} \Big[4\kappa \left(\tfrac{L}{2} + \epsilon_1\right) \cos\theta_i - 4\varphi \left(\tfrac{l}{2} + \epsilon_2\right) \sin\theta_i\Big] \Big\} d_{in} + (-1)^{\lfloor \frac{n}{2} \rfloor} \Big[4\kappa \left(\tfrac{L}{2} + \epsilon_1\right) \sin\theta_i + 4\varphi \left(\tfrac{l}{2} + \epsilon_2\right) \cos\theta_i\Big] \Big\} r_{in}; \end{aligned}$$

Let $C = \cos\theta_i$ and $S = \sin\theta_i$, then

$$d_{in} = \frac{4\kappa \left(\frac{L}{2} + \epsilon_1\right) C - 4\varphi \left(\frac{l}{2} + \epsilon_2\right) S}{\Big[4\kappa \left(\frac{L}{2} + \epsilon_1\right) C - 4\varphi \left(\frac{l}{2} + \epsilon_2\right) S\Big]^2 + \Big[4\kappa \left(\frac{L}{2} + \epsilon_1\right) S + 4\varphi \left(\frac{l}{2} + \epsilon_2\right) C\Big]^2}$$

and

$$r_{in} = \frac{\Big[4\kappa \left(\frac{L}{2} + \epsilon_1\right) S + 4\varphi \left(\frac{l}{2} + \epsilon_2\right) C\Big]^2}{\Big[4\kappa \left(\frac{L}{2} + \epsilon_1\right) C - 4\varphi \left(\frac{l}{2} + \epsilon_2\right) S\Big]^2 + \Big[4\kappa \left(\frac{L}{2} + \epsilon_1\right) S + 4\varphi \left(\frac{l}{2} + \epsilon_2\right) C\Big]^2}$$

where $\kappa = (1-(-1)^n)/2$ and $\varphi = (1+(-1)^n)/2$.

In order for the closest point on 8 line segments of the boundary to avoid kth disk shaped obstacle with the center $(o_{1k}, o_{2k}), k \in \mathbb{N}$, the following obstacle avoidance function is designed:

$$O_{ik}(\mathbf{x}) = \frac{1}{2}\left((X_{in} - o_{1k})^2 + (Y_{in} - o_{2k})^2 - r_{ok}^2\right). \tag{4}$$

Since only the outer line segments of A_0 are utilized in obstacle avoidance, the 8 lines inside are ignored due to maintaining rigid formation throughout the motion. Therefore the i and the n values in equation (4) can be generalized to $n = i + 1 - 4\lfloor \frac{i}{4} \rfloor$ and $i \in \{1,2,3,4\}$, where i and n represent the ith unit and its respective nth line segment.

3.4. Modulus bounds on velocity

The steering angle and linear speed of the compartmentalized robot A_0 must be limited for safety and which are observed through its units. As A_1 is the leader and to upkeep the formation of A_0, the values of the translational and rotational velocities of A_i for $i = \{2,3,4\}$ are $v_1 = v_2 = v_3 = v_4 = v_0$, $\omega_1 = \omega_2 = \omega_3 = \omega_4 = \omega_0$, $\phi_1 = \phi_2 = \phi_3 = \phi_4 = \phi_0$ respectively. If the maximum speed is $v_{max} > 0$ and maximum steering angle ϕ_{max} angle satisfies $0 < \phi_{max} < \frac{\pi}{2}$ then, the additional dynamical constraints imposed on the translational and the rotational velocities of A_1 (and hence the other units) are as follows:

(i) $|v_1| \le v_{max}$ where v_{max} is the maximal achievable speed of A_1.
(ii) $|\omega_1| \le |v_1|/|\rho_{min}| \le |v_{max}|/|\rho_{min}|$. This is obtained from $v_1^2 \ge \rho_{min}^2 \omega_1^2$ and ρ_{min} the minimum turning radius given by $\rho_{min} = L/\tan\phi_{max}$. The steering angle is bounded to ϕ_1 to $|\phi_1| \le \phi_{max}$, whereby ϕ_{max} is the *maximum steering angle* of A_1.

The only way such mechanical constraints and restrictions can be treated within LbCS is through the design of an artificial obstacle corresponding to each singularity [17]. Therefore, the composition of artificial obstacles again forms the basis for handling system singularities such as the constraint to steering angles of the mobile robotic units in this research paper. Avoidance of the following artificial obstacles guarantees that A_1 will operate within the desired limitations;

$$AO_1 = v_1 \in \mathbb{R} : v_1 \le v_{max} \text{ or } v_1 \ge v_{max},$$

$$AO_2 = \omega_1 \in \mathbb{R} : \omega_1 \le v_{max}/|\rho_{min}| \text{ or } \omega_1 \ge v_{max}/|\rho_{min}|.$$

Since the velocities of A_i for $i = 2,3,4$ are exactly the same as that of A_1 for all $t \ge 0$, the above restrictions will also be applicable to A_i for $i = 2,3,4$.

To avoid these obstacles the avoidance functions as derived in [17] are adopted:

$$U_1(x) = \frac{1}{2}\left(v_{max}^2 - v_1^2\right), \tag{5a}$$

$$U_2(x) = \frac{1}{2}\left(\frac{v_{max}^2}{\rho_{min}^2} - \omega_1^2\right). \tag{5b}$$

Both (5a) and (5b) ensures that the restrictions on translational velocity v_1 and the steering angle ϕ_1 are adhered to respectively.

4. Construction of nonlinear controllers

This section defines the Lyapunov function from which the control laws are derived. The following control/tuning parameters are introduced:

(i) $\alpha > 0$, for convergence of A_1 to the target,
(ii) $\beta_r > 0, r = 1,2$, to avoid the artificial obstacles associated with dynamic constraints,
(iii) $\gamma_{ik} > 0, i \in \{1,2,3,4\}$ and $k \in \mathbb{N}$, for avoidance of kth disk - shaped obstacle.

Using these parameters the Lyapunov Function for system (1) is designed as follows:

$$L(\mathbf{x}) = \alpha V(\mathbf{x}) + F(\mathbf{x})\left[\frac{\beta_1}{U_1(\mathbf{x})} + \frac{\beta_2}{U_2(\mathbf{x})} + \sum_{k=1}^{p}\sum_{i=1}^{4}\frac{\gamma_{ik}}{O_{ik}(\mathbf{x})}\right]. \tag{6}$$

The controllers for the robotic system are the time difference of various components of $L(\mathbf{x})$ along a solution of the dynamic system (1) and forced to be at least semi-negative definite. After carrying out necessary substitutions, suppressing $\mathbf{x}$ and using the convergence parameters, $\delta_1, \delta_2 > 0$, the controllers of the leader unit A_1 are of the form:

Theorem 4.1. *Consider a compartmentalized robot A_0 and its sub units A_i, $i \in \{1,2,3,4\}$, the motion of which is governed by the ODE's described by system (1). The objective is to assign A_1 as the leader and generate convergence to the target while maintaining a prescribed rigid formation with collision free maneuvers. Utilizing the attractive and repulsive field functions, the acceleration based controllers for A_0, which is governed by the leader A_1 are:*

$$\left.\begin{aligned}\sigma_{11} &= -\left(\delta_1 v_1 + \frac{\partial L}{\partial x_1}\cos\theta_1 + \frac{\partial L}{\partial y_1}\sin\theta_1\right) \Big/ \left(1 + F\frac{\beta_1}{U_1^2}\right), \\ \sigma_{12} &= -\left(\delta_2 \omega_1 - \frac{\partial L}{\partial x_1}\frac{L}{2}\sin\theta_1 + \frac{\partial L}{\partial y_1}\frac{l}{2}\cos\theta_1 + \frac{\partial L}{\partial \theta_1}\right) \Big/ \left(1 + F\frac{\beta_2}{U_2^2}\right).\end{aligned}\right\} \quad (7)$$

The acceleration controllers in (7) are only for the leader car-like robot A_1. The compartmentalized robot A_0's convergence to the target is facilitated by one of its units, which is the leader A_1. Since the other units A_i for $i \in \{2,3,4\}$ are in a rigid formation with the leader, they also converge to the target at the same speed as A_1, hence ensuring convergence of the compartmentalized robot A_0 to its target.

5. Stability analysis

Theorem 5.1. *Let $D(L_{(1)}(\mathbf{x})) = \{x \in \mathbb{R}^{5n} : U_r(\mathbf{x}) > 0, r \in \{1,2\}, O_{ik}(\mathbf{x}) > 0, \forall i = 1,2,3,4, k \in \mathbb{N}\}$. If a fixed point $\mathbf{x_1^*} = (P_{11}, P_{12}, \theta_1, v_1, \omega_1) \in \mathbb{R}^5$ is an equilibrium point of A_0, governed by the leader A_1 then $\mathbf{x_e} = \mathbf{x_1^*} \in D(L_{(1)}(\mathbf{x}))$ is the point of stability for system (1).*

Proof. The Lyapunov Function $L(\mathbf{x})$ of system (1) is considered to be defined, positive and continuous over the domain $D(L_{(1)}(\mathbf{x}))$, then it can be proven that $L_{(1)}(\mathbf{x})$ accomplishes the following properties:

1. $L_{(1)}(\mathbf{x})$ is defined, continuous, and positive over the domain $D(L_{(1)}(\mathbf{x}))$ in the locality of the equilibrium point $\mathbf{x_e}$ of system (1),
2. $L_{(1)}(\mathbf{x_e}) = 0$ since $V(\mathbf{x_e}) = 0$ and $F(\mathbf{x_e}) = 0$,

$$\begin{aligned} L(\mathbf{x_e}) &= \alpha V(\mathbf{x_e}) + F(\mathbf{x_e})\left[\frac{\beta_1}{U_1(\mathbf{x_e})} + \frac{\beta_2}{U_2(\mathbf{x_e})} + \sum_{k=1}^{p}\sum_{i=1}^{4}\frac{\gamma_{ik}}{O_{ik}(\mathbf{x_e})}\right] \\ &= \alpha(0) + 0\left[\frac{\beta_1}{U_1(\mathbf{x_e})} + \frac{\beta_2}{U_2(\mathbf{x_e})} + \sum_{k=1}^{p}\sum_{i=1}^{4}\frac{\gamma_{ik}}{O_{ik}(\mathbf{x_e})}\right] \\ &= 0, \end{aligned}$$

3. $L_{(1)}(\mathbf{x}) > 0$ for all $\mathbf{x} \in D(L_{(1)}(\mathbf{x})/\mathbf{x_e}$ since $V(\mathbf{x}) > 0,\ F(\mathbf{x}) > 0$ along with $U_{1r}(\mathbf{x}) > 0, r \in \{1,2\}, O_{ik}(\mathbf{x}) > 0, \forall i = 1,2,3,4, k \in \mathbb{N}$ on the domain $D(L_{(1)}(\mathbf{x}))$.

The following time derivative, semi negative definite function of $L_1(\mathbf{x})$ is obtained by substituting the controllers in Theorem 5.1 and the ODE's for system (1) in (6)

$$\dot{L}_{(1)}(\mathbf{x}) = \frac{\partial L}{\partial x_1}\dot{x}_1 + \frac{\partial L}{\partial y_1}\dot{y}_1 + \frac{\partial L}{\partial \theta_1}\dot{\theta}_1 + \frac{\partial L}{\partial v_1}\dot{v}_1 + \frac{\partial L}{\partial \omega_1}\dot{\omega}_1$$

Given the convergence parameters $\delta_1, \delta_2 > 0$, then

$$\dot{L}_{(1)}(\mathbf{x}) = -\delta_1 v_1^2 - \delta_2 \omega_1^2 \leq 0.$$

Consequently $\dot{L}_{(1)}(\mathbf{x}) < 0$, for all $\mathbf{x} \in D(L_{(1)}(\mathbf{x})$ and $\dot{L}_{(1)}(\mathbf{x_e}) = 0$. Furthermore $L_{(1)}(\mathbf{x}) \in (D(L_{(1)}(\mathbf{x}))$, therefore for the system (1), $L_{(1)}(\mathbf{x})$ is designated as its Lyapunov Function and $\mathbf{x_e}$ a stable equilibrium point over the domain $D(L_{(1)}(\mathbf{x})$.

It is also worth mentioning that the establishment of a unique domain $D(L_{(1)}(x))$ removes any possible singularities of the Lyapunov function. Here the $L_{(1)}(\mathbf{x})$ is defined, continuous, and positive over the domain $D(L_{(1)}(\mathbf{x}))$ in the neighborhood of the equilibrium point. Also the inherent nature of $L_{(1)}(\mathbf{x})$ prevents it from being undefined since the avoidance functions can never be equal to zero. The computer simulations authenticate the design of the controllers, the stability analysis for the robotic system, and the validity of the Lyapunov-based Control Scheme (LbCS).

6. Simulations

This section demonstrates the simulation results for the compartmentalized robot and numerically verifies the stability results obtained from the Lyapunov function.

6.1. Scenario 1

The first scenario for motion planning captures a simple situation that illustrates the effectiveness of the control laws by considering a fixed circular obstacle in the workspace. Here the compartmentalized robot can be seen as a garbage collecting robot, traversing from one place of collection to another. Each unit whereby is assigned to collect different types of household refuse such as solid waste, recyclable waste, organic waste and hazardous waste. Fig. 5 shows the snapshots captured at different times of evolution of A_0 maneuvering from its initial point of location to its target point, steering clear off the fixed obstacle in its path. This scenario also

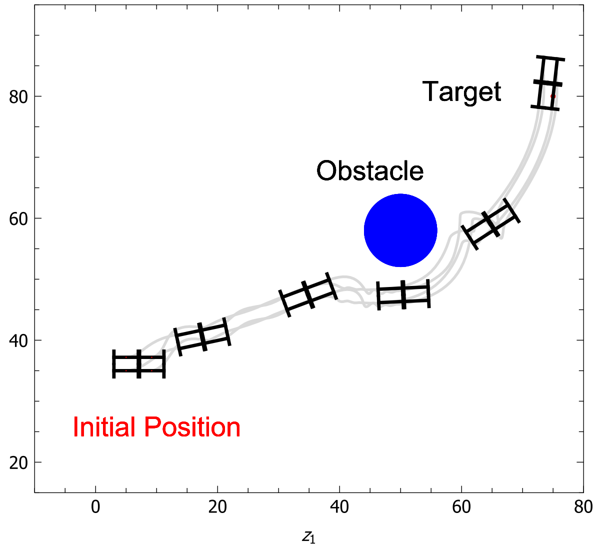

Fig. 5. *Scenario* 1. Integrated snapshot showing the motion of A_0 at different times, $t \geq 0$.

Table 1
Initial states and various parameter values.

Initial position	$(x_0, y_0) = (5, 35)$ m.
Initial orientation	$(\theta_0) = 0$ rad.
Initial linear (translational) velocity	$(v_0) = 0$ m/s.
Initial angular (rotational) velocity	$(\omega_0) = 0$ rad/s.
Length of Vehicle	$L = 4$ m.
Width of Vehicle	$l = 2$ m.
Radius of Circular Protective region	$r_v = 2.37$ m.
Target center	$(P_{11}, P_{12}) = (75, 80)$ m
Radius of target	$r_T = 0.4$ m
Target center	$(o_{11}, o_{12}) = (50, 58)$ m
Radius of obstacle	$r_o = 6$ m
Workspace dimensions	$0 \leq z_1 \leq 100$, $0 \leq z_2 \leq 100$.
Number of compartmentalized robots	$n = 1$.
Number of compartments in the Unit	$i = 4$.
Number of obstacles	Scenario 1: $k = 1$
	Scenario 2: $k = 6$
	Scenario 3: $k = 12$
Clearance Parameters	$\epsilon_1 = 0.1$ m, $\epsilon_2 = 0.1$ m.
Control Parameters	$\beta_1 = 0.001, \beta_2 = 0.001$.
	Scenario 1: $\alpha = 0.00002$.
	Scenario 2: $\alpha = 0.005$.
	Scenario 3: $\alpha = 0.005$.
Convergence Parameters	Scenario 1: $\delta_1 = 10, \delta_2 = 10$.
	Scenario 2: $\delta_1 = 1, \delta_2 = 1$.
	Scenario 3: $\delta_1 = 1, \delta_2 = 1$.

verifies the effectiveness of the MDT technique. The initial and final position and states, the numerical values of the various parameters, restrictions and limitations due to vehicle dynamics for scenarios 1, 2, 3 are provided in Table 1. Under the initial parameters, the control laws verified that the system converges to the equilibrium state. Fig. 6(a) shows the time derivatives of the Lyapunov function along the system trajectories. It indicates the periods in which the controllers in (7) decrease or increase their energy loss with respect to time at which the units avoid the obstacle or converge to its target. The rigid formation is maintained throughout the motion as the distance of A_i for $i = 2, 3, 4$ with respect to the leader A_1 is fixed as shown in 6(b). Fig. 7(a) shows the translational velocities and Fig. 7(b) shows the rotational velocities of the vehicles. Whereas, Fig. 7(c) and Fig. 7(d) show the translational and rotational acceleration of the vehicles, respectively, which clearly reveal the convergent property of the navigation laws. Looking at the figures it can be deduced that A_1 slowed down while avoiding the fixed obstacle and after avoidance it again gains speed and then slows down on approach to the target.

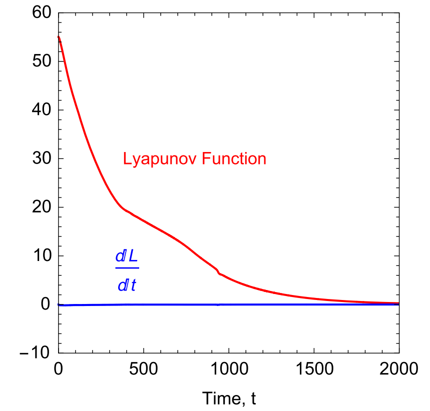

(a) Lyapunov Function and its time derivative.

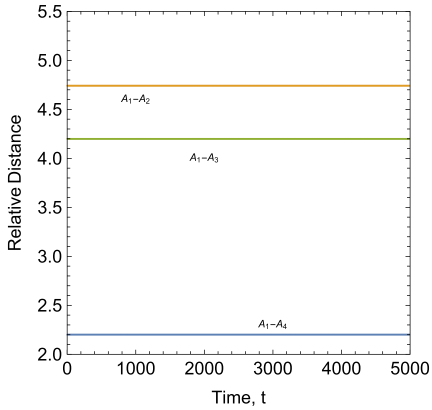

(b) Relative distance of A_i from A_1.

Fig. 6. *Scenario* 1. (a) Monotonically decreasing Lyapunov function. (b) The distances between the compartments are constant.

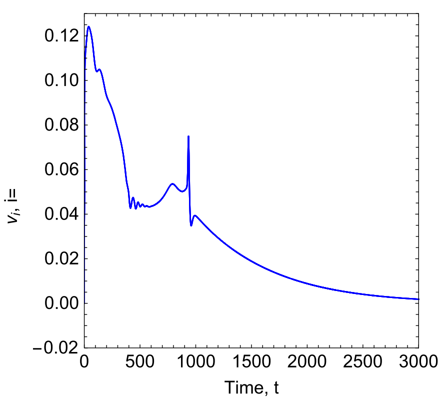

(a) Translational velocity.

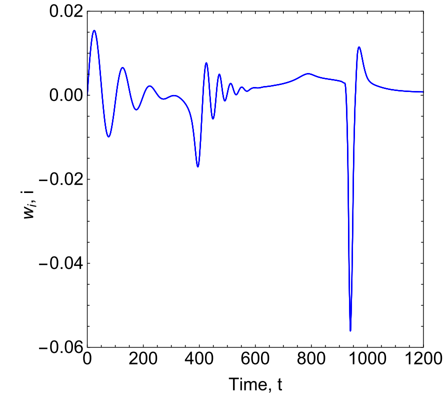

(b) Rotational velocity.

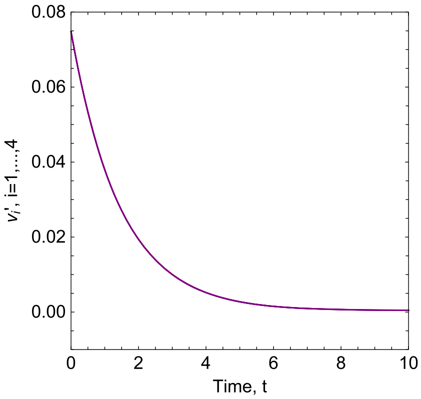

(c) Translational acceleration.

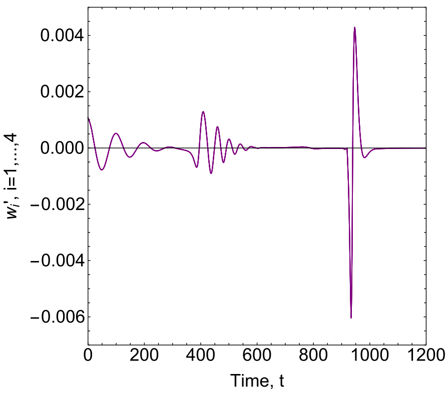

(d) Rotational acceleration.

Fig. 7. *Scenario* 1. (a) Translational velocity υ of A_0. (b) Rotational velocity ω of A_0. (c) Translational acceleration $\dot{\upsilon}$ of the A_0. (d) Rotational acceleration $\dot{\omega}$ of A_0.

6.2. Scenario 2

The second scenario illustrates the effectiveness of the control laws in presence of randomly placed circular obstacles of random sizes. It could be seen as an application of automated robots that are designed for transporting supplies of goods, search and rescue after disaster and attack of enemies. Fig. 8 shows the compartmentalized robot A_0, captured with snapshots at different times of evolution, moving from an initial state to the target, avoiding random sized obstacles placed randomly in the workspace. The effectiveness of MDT is verified here as the closest point of any line segment of the rectangular protective region and a fixed obstacle

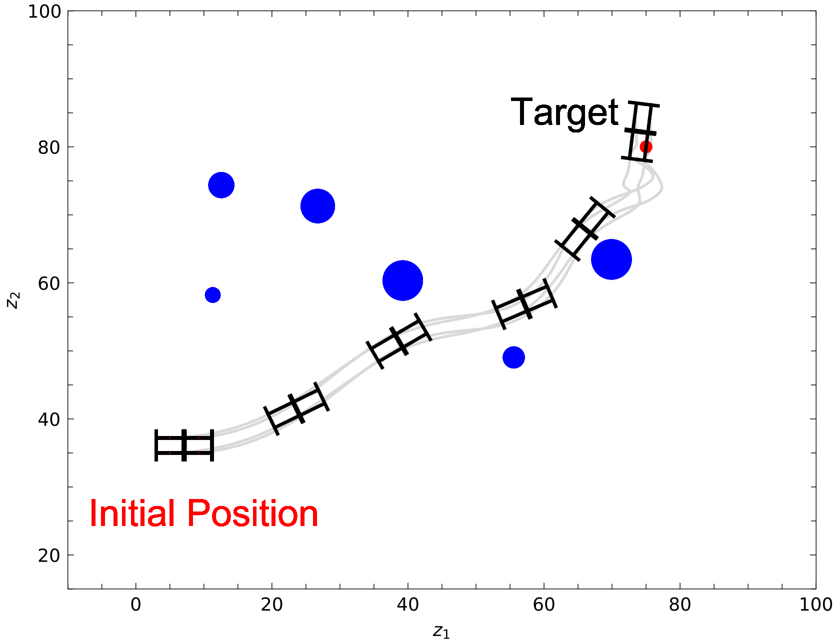

Fig. 8. *Scenario* 2. Shows the trajectory of A_0 around the obstacles. Integrated snapshot showing the motion of the units.

avoids that obstacle while A_0 converges to its target. Table 1 furnishes numerical values of parameters, the initial and final states of A_0, restrictions and limitations due to vehicle dynamics and workspace. The controllers guarantee convergence of the system to the equilibrium state. Figs. 9(a) and 9(b) show the translational and rotational velocity of the leader unit A_1. Figs. 9(c) and 9(d) illustrate the evolution of nonlinear controllers of the leader, A_1. The peaks and the spikes in the graphs show maximum energy dissipation and obstacle avoidance by the compartmentalized robot.

6.3. Scenario 3

The third scenario is the motion control of A_0 in presence of 12 randomly placed circular obstacles. Scenarios 2 and 3 are similar except that the number of obstacles has increased. It could be an application of a compartmentalized robot providing medical assistance to a quarantined area such as the global corona virus pandemic. Examples of medical assistance include taking patient's vitals, laser disinfectants, food and medication and broadcasting public messages about precautionary measures during the pandemic. Fig. 10 shows collision free trajectory of A_0, captured with snapshots at different times of evolution. The behavior of the controllers along the trajectory of A_0 can be seen in Figs. 11(a), 11(b), 11(c), and 11(d). A rise in the controller values at specific times indicates obstacle avoidance by the system. Nevertheless, just after the avoidance, the controllers are decreased in magnitude to the proximity of the time axis, which significantly hints the asymptotic behavior of the controllers.

7. Discussion

Individual robots that combine to form one larger, cooler automaton have been a mainstay of science fiction for decades. Morphing robots is finally outgrowing the limits of fiction and finding its way into reality. The concept of compartmentalization that originates from cells, the building blocks of life, is treated as a MPC problem of a car-like robot by utilizing the LbCS, an emerging artificial potential field technique. A set of continuous, time-invariant, non-linear acceleration controllers of a compartmentalized robot is formulated to enable the robot's navigation in an environment that is cluttered with obstacles. Simulation results shown in Figs. 5, 8 and 10 show the effectiveness of the controllers and robustness of the system for navigating in an environment dominated by obstacles.

There are different algorithms or techniques in literature to navigate a compartmentalized robot in unconstrained and constrained environments [32,33,38,39]. In [38] the motion control of a Mergeable Nervous System (MNS) robot is exhibited in a high-level logic that is unconstrained by the robot's shape and size. High-level commands are issued by the brain unit that is transmitted through the robot's nervous system [39]. The LbCS is mightily used over other motion control paradigms because mathematical functions associated with limitations, inequalities, and other mechanical restrictions associated with a robotic system are easier to design and integrate into the controllers. It also proves the stability and autonomously navigates the system. The systems presented in [38,39], compared to LbCS require sophisticated sensory - motor coordination. The motion control model for such robots is inhibited to a predetermined set of morphologies. The compartmentalized robot in this paper is in rigid formation. The tasks performed by the compartmentalized robot are mainly facilitated by only a single sub-unit, the leader. The other sub-units are not performing any tasks which can be an area of research in future.

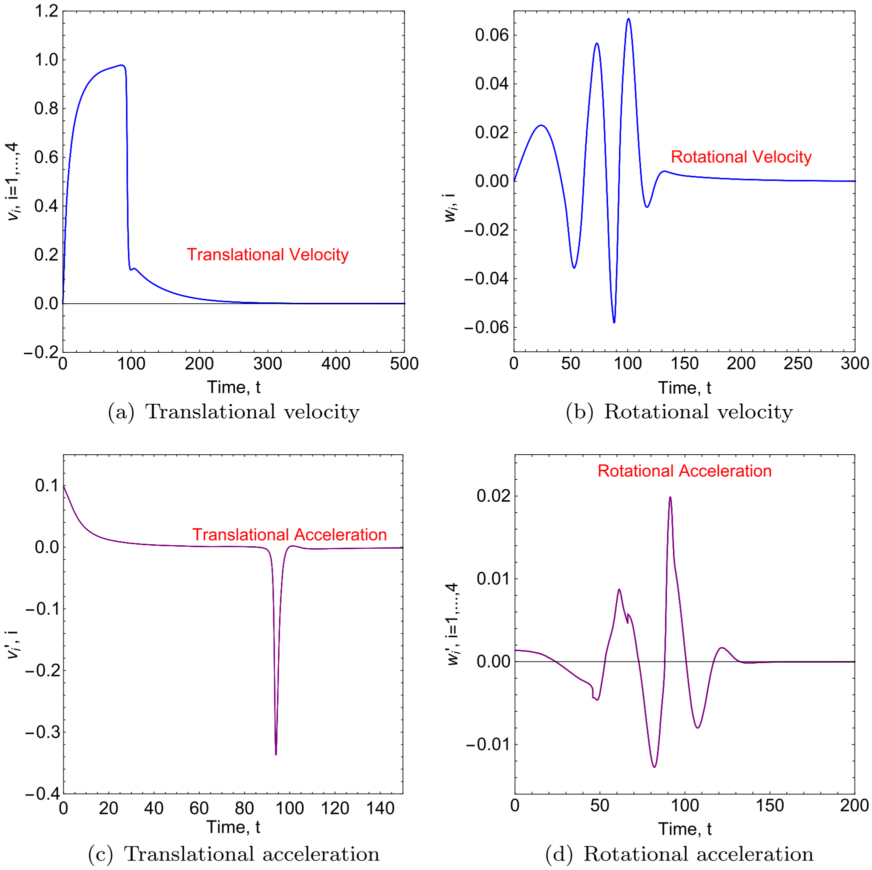

Fig. 9. *Scenario* 2. (a) Translational velocity v of A_0. (b) Rotational velocity ω of A_0. (c) Translational acceleration $\dot{v}$ of the A_0. (d) Rotational acceleration $\dot{\omega}$ of A_0.

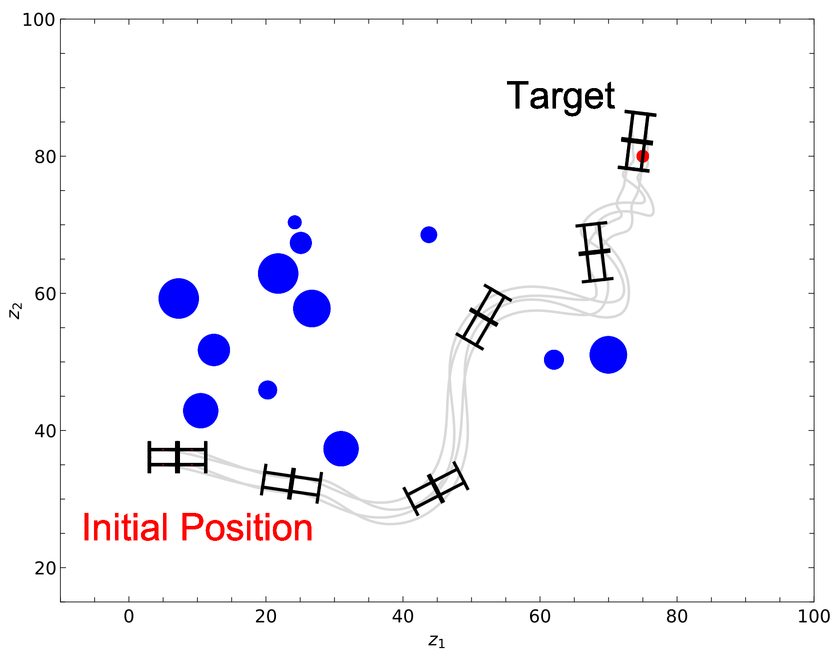

Fig. 10. *Scenario* 3. Shows the trajectory of A_0 around the obstacles. Integrated snapshot showing the motion of the units.

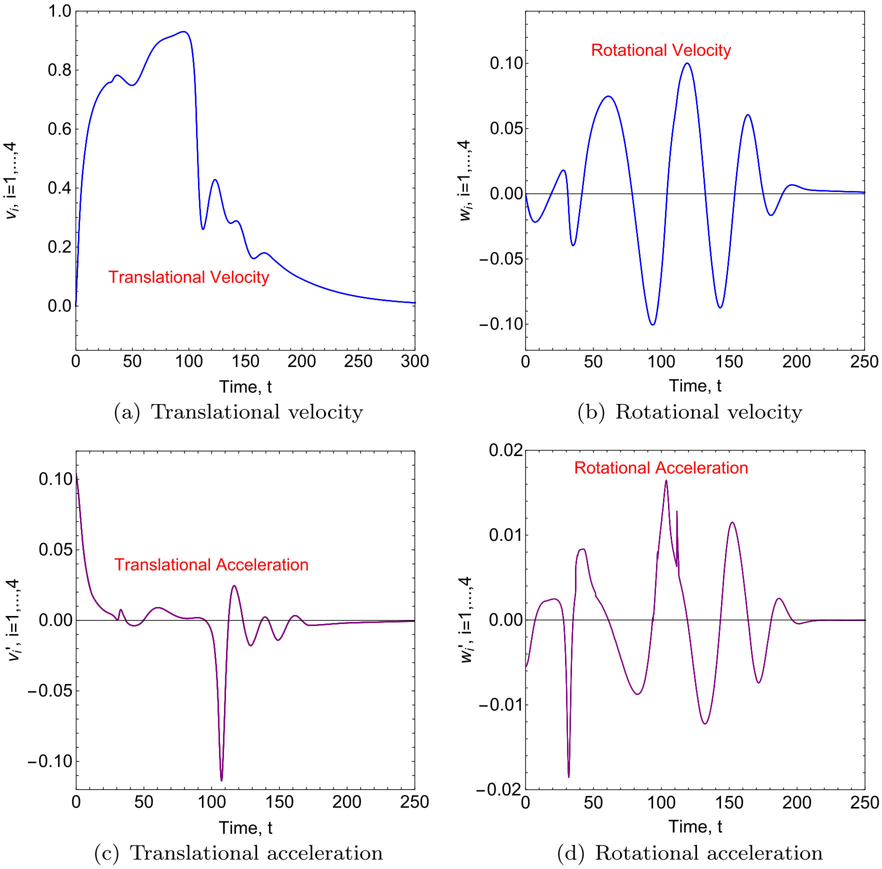

Fig. 11. *Scenario* 3. (a) Translational velocity v of A_0. (b) Rotational velocity ω of A_0. (c) Translational acceleration $\dot{v}$ of the A_0. (d) Rotational acceleration $\dot{\omega}$ of A_0.

8. Conclusion

A new set of continuous, time-invariant, non-linear acceleration controllers are designed using LbCS to solve the motion planning and control problem of a compartmentalized robot in an obstacle cluttered workspace. In presence of randomly fixed obstacles, the continuous acceleration-based controllers have efficaciously governed the compartmentalized robot to its target, facilitated by a designated leader. In order to maintain the formation of the compartmentalized robot, all the units in the compartmentalized robot converge to the target at the same velocity as the leader unit. One can clearly notice that from the initial state to the final state the units maintained their relative distance from the leader, which numerically proves that the car- like units maintains a rigid formation, which is an adaptation of globally rigid formation. The concept of minimum distance technique has been favorably applied for avoidance of obstacles. The nonlinear controllers are synthesized by utilizing the Lyapunov-based control strategy. The control laws introduced in this paper also verify the stability of the compartmentalized robot system. It has also been proved by Lyapunov's Direct Method and verified numerically by the computer simulations. To the best of the author's knowledge, there have been no works published so far where a compartmentalized robot is modeled within the LbCS as a motion planning and control problem. Such approach is motivated by the idea that the robots are not modeled for one particular task only. Designing compartmentalized robots gives complaisance to robots to adapt to their capabilities autonomously and to the changing task requirements. The applications are discussed as 3 scenarios in the simulation.

One of the limitations of this paper is the absence of any experimental verification. Only the theoretical exposition of LbCS is presented in this paper and is limited to showing the effectiveness of acceleration-based controllers numerically using computer simulations of exciting scenarios. It is practicable, however, for the commercial and other relevant sectors to include such controllers for the development of compartmentalized robots that could perform a sequence of industrial and other tasks.

Future work in this area will be directed along the same path having multiple units as a swarm model to be guided to the target. Also splitting the unit into its smaller compartments while carrying out different tasks in parallel and rejoining upon completion of the tasks. The concept of rotational leadership roles can also be considered.

Funding statement

This research did not receive any specific grant from funding agencies in the public, commercial, or not-for-profit sectors.

Author contribution statement

Bibhya Sharma, Avinesh Prasad: Conceived and designed the experiments; Analyzed and interpreted the data; Contributed reagents, materials, analysis tools or data; Wrote the paper.

Riteshni D. Karan: Analyzed and interpreted the data; Contributed reagents, materials, analysis tools or data; Wrote the paper.

Sandeep A. Kumar: Performed the experiments; Analyzed and interpreted the data; Contributed reagents, materials, analysis tools or data; Wrote the paper.

Declaration of competing interest

The authors declare that they have no known competing financial interests or personal relationships that could have appeared to influence the work reported in this paper.

Data availability statement

No data was used for the research described in the article.

References

[1] M.N.A. Wahab, S. Nefti-Meziani, A. Atyabi, A comparative review on mobile robot path planning: classical or meta-heuristic methods?, Annu. Rev. Control 50 (2020) 233–252, https://doi.org/10.1016/j.arcontrol.2020.10.001, https://www.sciencedirect.com/science/article/pii/S1367578820300675.
[2] R. Grandia, A. Taylor, A. Singletary, M. Hutter, A. Ames, Nonlinear model predictive control of robotic systems with control Lyapunov functions, 06 2020.
[3] A. Burhanudin, S. Supriyadi, M. Malik, Neural networks and behaviour based control for education botanical robot navigation, J. Phys. Conf. Ser. 1464 (2020) 012002, https://doi.org/10.1088/1742-6596/1464/1/012002.
[4] A. Talli, Modelling and Simulation of Industrial Robot Using Solid Works, 2021, pp. 173–182.
[5] G. Alderton, Making robots useful, Science 369 (2020) 930.10–932, https://doi.org/10.1126/science.369.6506.930-j.
[6] P. Machado, J. Bonnell, S. Brandenburg, J.F. Ferreira, D. Portugal, M. Couceiro, Robotics Use Case Scenarios, 2020, p. 152.
[7] J.L. Farrugia, S.G. Fabri, Swarm robotics for object transportation, in: 2018 UKACC 12th International Conference on Control (CONTROL), IEEE, 2018, pp. 353–358.
[8] P. Archana, Fire fighting robot using internet of robotic things, Int. J. Res. Appl. Sci. Eng. Technol. 9 (2021) 3872–3879, https://doi.org/10.22214/ijraset.2021.35836.
[9] S. Chien, K. Wagstaff, Robotic space exploration agents, Sci. Robot. 2 (2017) eaan4831, https://doi.org/10.1126/scirobotics.aan4831.
[10] S. Arora, The jugular foramen: compartmentalisation, J. Evol. Med. Dent. Sci. 5 (2016) 3483–3485, https://doi.org/10.14260/jemds/2016/804.
[11] N. Kshetri, A survey on computer ethics (w.r.t. artificial intelligence, robot weaponry, fuzzy systems, autonomous vehicles), 02 2021.
[12] K. Tiwari, N. Chong, Multi-robot systems, 2020, pp. 159–169.
[13] A.M. Varghese, V.R. Jisha, Motion planning and control of an autonomous mobile robot, in: 2018 International CET Conference on Control, Communication, and Computing (IC4), 2018, pp. 17–21.
[14] R. França, A. Monteiro, R. Arthu, Y. Iano, The evolution of robotic systems, 2020, pp. 1–20.
[15] R. Fierro, L. Chaimowicz, V. Kumar, Multi-robot cooperation, in: Autonomous Mobile Robots, CRC Press, 2018, pp. 417–460.
[16] L. Fang, P.J. Antsaklis, Decentralized formation tracking of multi-vehicle systems with nonlinear dynamics, in: 14th Mediterranean Conference on Control and Automation, Ancona, Italy, 2016.
[17] B. Sharma, J. Vanualailai, A. Prasad, Formation control of a swarm of mobile manipulators, Rocky Mt. J. Math. (2011) 909–940.
[18] L. Consolini, F. Morbidi, D. Prattichizzo, M. Tosques, Stabilization of a hierarchical formation of unicycle robots with velocity and curvature constraints, IEEE Trans. Robot. 25 (5) (2009) 1176–1184.
[19] T. Ikeda, J. Jongusuk, T. Ikeda, T. Mita, Formation control of multiple nonholonomic mobile robots, Electr. Eng. Jpn. 157 (3) (2006) 81–88.
[20] B. Wohlfender, Studies on mechatronics: autonomous collaborative vehicles, 2010.
[21] L.E. Barnes, A Potential Field Based Formation Control Methodology for Robot Swarms, University of South Florida, 2008.
[22] X. Chen, Y. Li, Stability on adaptive nn formation control with variant formation patterns and interaction topologies, Int. J. Adv. Robot. Syst. 5 (1) (2008) 8.
[23] K. Kanjanawanishkul, Formation control of mobile robots: survey, UBU Eng. J. 4 (1) (2016) 50–64.
[24] E. Masehian, D. Sedighizadeh, Classic and heuristic approaches in robot motion planning–a chronological review, World Acad. Sci., Eng. Technol. 23 (5) (2007) 101–106.
[25] B. Oommen, S. Iyengar, N. Rao, R. Kashyap, Robot navigation in unknown terrains using learned visibility graphs. Part I: The disjoint convex obstacle case, IEEE J. Robot. Autom. 3 (6) (1987) 672–681.
[26] C. Cai, S. Ferrari, Information-driven sensor path planning by approximate cell decomposition, IEEE Trans. Syst. Man Cybern., Part B, Cybern. 39 (3) (2009) 672–689.
[27] X. Yang, M. Moallem, R.V. Patel, A layered goal-oriented fuzzy motion planning strategy for mobile robot navigation, IEEE Trans. Syst. Man Cybern., Part B, Cybern. 35 (6) (2005) 1214–1224.
[28] Y.-J. Liu, Q. Zeng, S. Tong, C.P. Chen, L. Liu, Adaptive neural network control for active suspension systems with time-varying vertical displacement and speed constraints, IEEE Trans. Ind. Electron. 66 (12) (2019) 9458–9466.
[29] M.Z. Zgurovsky, Y.P. Zaychenko, Fuzzy neural networks in classification problems, in: The Fundamentals of Computational Intelligence: System Approach, Springer, 2016, pp. 179–219.
[30] P. Bhattacharya, M.L. Gavrilova, Roadmap-based path planning-using the Voronoi diagram for a clearance-based shortest path, IEEE Robot. Autom. Mag. 15 (2) (2008) 58–66.
[31] X. Fan, Y. Guo, H. Liu, B. Wei, W. Lyu, Improved artificial potential field method applied for autonomous underwater vehicle path planning, Math. Probl. Eng. 2020 (2020).
[32] B. Yousra, E.A. Ahmed, Collection and transport of waste types by compartmentalised vehicles, in: 2020 5th International Conference on Logistics Operations Management (GOL), 2020, pp. 1–5.
[33] A. Ribeiro, J. Conesa-Muñoz, Multi-robot Systems for Precision Agriculture, 2021, pp. 151–175.
[34] G. Baldassarre, V. Trianni, M. Bonani, F. Mondada, M. Dorigo, S. Nolfi, Self-organized coordinated motion in groups of physically connected robots, IEEE Trans. Syst. Man Cybern., Part B, Cybern. 37 (2007) 224–239, https://doi.org/10.1109/TSMCB.2006.881299.

[35] J.-H. Hofmeyr, Kinetic modelling of compartmentalised reaction networks, https://doi.org/10.31219/osf.io/5as9h, 04 2020.
[36] B. Jolly, C. Liu, A generalized kinetic model for compartmentalization of organometallic catalysis, 2021.
[37] R. Kourist, J. Sabín, Compartmentalization in Biocatalysis, 2021, pp. 89–112.
[38] N. Mathews, A. Christensen, R. O'Grady, F. Mondada, M. Dorigo, Mergeable nervous systems for robots, Nat. Commun. 8 (12 2017), https://doi.org/10.1038/s41467-017-00109-2.
[39] W. Savoie, T. Berrueta, Z. Jackson, A. Pervan, R. Warkentin, S. Li, T. Murphey, K. Wiesenfeld, D. Goldman, A robot made of robots: emergent transport and control of a smarticle ensemble, Sci. Robot. 4 (2019), eaax4316, https://doi.org/10.1126/scirobotics.aax4316.
[40] J. Raj, K. Raghuwaiya, J. Vanualailai, Collision avoidance of 3d rectangular planes by multiple cooperating autonomous agents, J. Adv. Transp. 2020 (2020) 1–13, https://doi.org/10.1155/2020/4723687.
[41] R. Chand, R.P. Chand, M. Assaf, P.R. Naicker, S.V. Narayan, A.F. Hussain, Embedded fpga-based motion planning and control of a dual-arm car-like robot, in: 2022 IEEE 7th Southern Power Electronics Conference (SPEC), 2022, pp. 1–6.
[42] R.P. Chand, R. Chand, M. Assaf, P.R. Naicker, S.V. Narayan, Acceleration feedback controller processor design of a kids personal transporter (kpt), in: 2022 IEEE 7th Southern Power Electronics Conference (SPEC), 2022, pp. 1–6.
[43] R.P. Chand, R. Chand, M. Assaf, S.V. Narayan, P.R. Naicker, V. Kapadia, Acceleration feedback controller processor design of a segway, in: 2022 IEEE 7th Southern Power Electronics Conference (SPEC), 2022, pp. 1–6.
[44] B.N. Sharma, J. Raj, J. Vanualailai, Navigation of carlike robots in an extended dynamic environment with swarm avoidance, Int. J. Robust Nonlinear Control 28 (2) (2018) 678–698.